

## Magnetic field influence on the proximity effect at $\text{YBa}_2\text{Cu}_3\text{O}_7/\text{La}_{2/3}\text{Ca}_{1/3}\text{MnO}_3$ superconductor/half-metal interfaces

C. Visani,<sup>1,2,\*</sup> F. Cuellar,<sup>1,2</sup> A. Pérez-Muñoz,<sup>3</sup> Z. Sefrioui,<sup>3</sup> C. León,<sup>3</sup> J. Santamaría,<sup>1,2,3</sup> and Javier E. Villegas<sup>1,2,†</sup>

<sup>1</sup>Unité Mixte de Physique CNRS/Thales, 1 avenue A. Fresnel, 91767 Palaiseau, France

<sup>2</sup>Université Paris Sud 11, 91405 Orsay, France

<sup>3</sup>GFMC, Departamento Física Aplicada III, Universidad Complutense de Madrid, 28040 Madrid, Spain

(Received 8 June 2015; revised manuscript received 1 July 2015; published 31 July 2015)

We experimentally study the superconducting proximity effect in high-temperature superconductor/half-metallic ferromagnet  $\text{YBa}_2\text{Cu}_3\text{O}_7/\text{La}_{2/3}\text{Ca}_{1/3}\text{MnO}_3$  junctions, using conductance measurements. In particular, we investigate the magnetic-field dependence of the spectroscopic signatures that evidence the long-range penetration of superconducting correlations into the half-metal. Those signatures are insensitive to the applied field when this is below the ferromagnet's saturation fields, which demonstrates that they are uncorrelated with its macroscopic magnetization. However, the application of more intense fields progressively washes away the fingerprint of long-range proximity effects. This is consistent with the fact that the well-known magnetic inhomogeneities at the  $c$ -axis  $\text{YBa}_2\text{Cu}_3\text{O}_7/\text{La}_{2/3}\text{Ca}_{1/3}\text{MnO}_3$  interface play a role in the proximity behavior.

DOI: [10.1103/PhysRevB.92.014519](https://doi.org/10.1103/PhysRevB.92.014519)

PACS number(s): 74.45.+c, 74.78.Fk

Ferromagnetic order and singlet superconductivity are incompatible, because the magnetic exchange field breaks apart the conventional opposite-spin Cooper pairs. For this reason, the superconducting proximity effect is generally short ranged in superconductor/ferromagnet (S/F) structures [1]. However, a long-range propagation of superconducting correlations into an F is expected if a conversion from “opposite-spin singlet” to “equal-spin triplet” pairing occurs at the S/F interface [2]. Equal-spin triplets are immune to the exchange field, and can propagate into ferromagnets over the same long distance as singlets into normal metals [2]. During recent years, various experiments have found long-range proximity effects and Josephson coupling in specific S/F systems [3–9], which have been interpreted in terms of singlet-to-triplet conversion. Besides its fundamental interest, equal-spin triplet superconductivity may yield novel technological applications within the field of spintronics [10]. In this sense, half-metal ferromagnets are especially interesting, because the triplet superconducting condensate must be fully spin polarized in these materials [11].

Among the half-metal-based S/F systems in which long-range proximity effects have been observed, all-oxide heterostructures that combine manganites ( $\text{La}_x\text{Ca}_{1-x}\text{MnO}_3$  or  $\text{La}_x\text{Sr}_{1-x}\text{MnO}_3$ ) and cuprate superconductors have received continued attention [8,9,12–19]. From the early hints based on the critical temperature ( $T_C$ ) measurements in S/F superlattices [14,20], to the more recent spectroscopic [8,9,19] and Josephson current measurements in S/F junctions [21], various experiments have provided evidence for long-range superconducting proximity effects in half-metallic manganites. However, the physical origin of the singlet-to-triplet conversion—which could be different for each cuprate/manganite combination—has not been identified. As theoretically shown for generic S/F systems, the singlet-to-triplet conversion can be produced by interfacial magnetic

inhomogeneities [2,22–24]. This was experimentally confirmed in ordinary (not half-metallic) ferromagnets via the introduction of artificial “magnetic inhomogeneities” [5,7]. In the case of half-metallic ferromagnets, the singlet-to-triplet conversion can be explained [11,25–27] by two subsequent processes—(i) spin mixing and (ii) spin flip—which arise from (i) spin dependent electron scattering and (ii) magnetic inhomogeneities or other sources of misalignments of the spin quantization axis at the interface (e.g. spin-orbit coupling effects [28–31]). Recent scanning tunneling microscopy (STM) experiments in  $a$ -axis  $\text{YBa}_2\text{Cu}_3\text{O}_7/\text{La}_{2/3}\text{Ca}_{1/3}\text{MnO}_3$  and  $\text{Pr}_{1.85}\text{Ce}_{0.15}\text{CuO}_4/\text{La}_{2/3}\text{Ca}_{1/3}\text{MnO}_3$  (PCCO/LCMO) bilayers found a strong magnetic-field dependence of the spectral features that constitute the fingerprint of the long-range proximity effect [19]. The observed magnetic-field dependence was considered evidence for the role of magnetic inhomogeneities in the long-range proximity effects in LCMO.

Motivated by that experiment in  $a$ -axis YBCO/LCMO [19], in this paper we study the field dependence of the proximity effects in heterostructures with a different YBCO crystalline orientation; in particular,  $c$ -axis YBCO/LCMO heterostructures. Earlier conductance measurements in this system showed spectral evidence for equal-spin Andreev reflection and long-range penetration of superconducting correlations into LCMO [9]. At variance with the observations by Kalcheim *et al.* [19], in the  $c$ -axis heterostructures studied here the spectral features that constitute the evidence for a long-range proximity effect are essentially insensitive to moderate magnetic fields (within the field range required to saturate the LCMO macroscopic magnetization). However, the application of increasingly stronger fields gradually washes away those spectral features. As discussed below, this behavior is consistent with the idea that the well-known magnetic inhomogeneities at the  $c$ -axis YBCO/LCMO interface play a role in the triplet condensate generation. However, the present experiments do not allow ruling out the concomitance of additional mechanisms.

The experiments were conducted in vertical microjunctions (junction areas ranging from  $\sim 5$  to  $100 \mu\text{m}^2$ ), which were

\*Present address: Department of Applied Physics, Yale University, New Haven, Connecticut 06511, USA.

†javier.villegas@thalesgroup.com

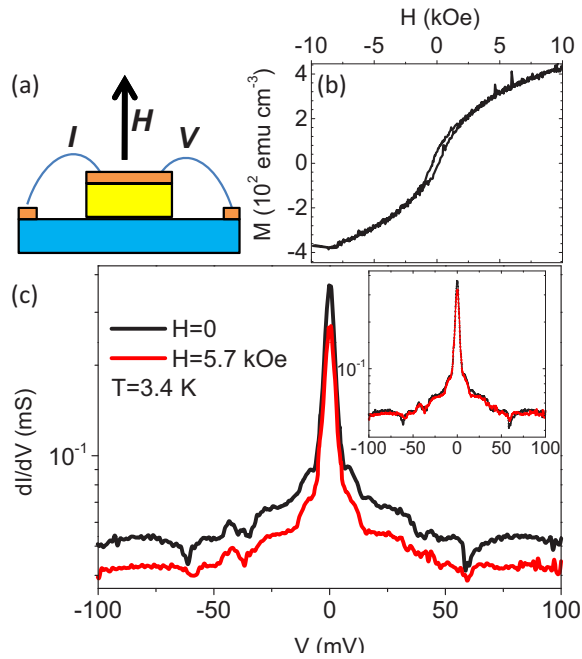


FIG. 1. (Color online) (a) Sketch of the vertical junction and applied field direction. (b) Hysteresis loop of a LCMO (15 nm)/STO// sample with the magnetic field applied perpendicular to the film plane and at  $T = 77$  K. (c) Differential conductance across a Au/YBCO (30 nm)/LCMO (30 nm)/STO// junction (area  $32 \mu\text{m}^2$ ), measured at  $T = 3.4$  K in the absence of magnetic field (black curve) and under  $H = 5.7$  kOe (red curve). In the main panel, the curves have been deliberately shifted vertically for clarity. The inset shows the raw data.

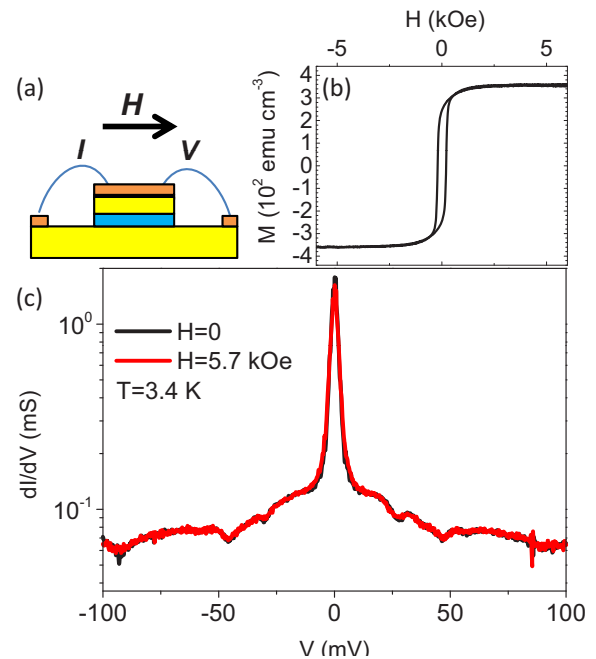


FIG. 2. (Color online) (a) Sketch of the vertical junction and applied field direction. (b) Hysteresis loop of a LCMO (15 nm)/YBCO (15 nm)/STO// bilayer, with the magnetic field applied parallel to the film plane and at  $T = 100$  K. (c) Differential conductance across a Au/YBCO (15 nm)/LCMO (12 nm)/YBCO (30 nm)/STO// junction (area  $64 \mu\text{m}^2$ ), measured at  $T = 3.4$  K in the absence of magnetic field (black curve) and under  $H = 5.7$  kOe (red curve).

fabricated as described elsewhere [9]. *c*-axis YBCO/LCMO bilayers and YBCO/LCMO/YBCO trilayers were grown on SrTiO<sub>3</sub> using high-pressure O<sub>2</sub> sputtering. The structural, magnetic, and superconducting properties of these heterostructures have been thoroughly characterized [32–35]. Vertical junctions (for transport measurements perpendicular to the heterostructure interfaces) were obtained via a series of lithography, etching, insulator, and Au deposition steps. Sketches of the junctions are displayed in Figs. 1(a), 2(a), and 3(a). Actual sample pictures and further details about sample fabrication can be found in Ref. [9]. The top and bottom electrodes are made of *ex situ* deposited Au. dc voltage biased  $I(V)$  measurements were done at various temperatures and magnetic fields, using the electrical probe configuration depicted in the sketches. The  $I(V)$  were numerically differentiated to obtain the conductance  $dI/dV$  shown in Figs. 1(c), 2(c), 3(b), and 3(c).

Qualitatively, the conductance vs bias in the absence of magnetic field is similar in all cases. The conductance curves show a pronounced zero-bias peak and a series of oscillations, which appear symmetrically for positive and negative bias [9]. These arise from McMillan-Rowell resonances [36,37] in the LCMO layer and Tomasch resonances [38] in YBCO, and constitute the evidence for long-ranged superconducting proximity effects in LCMO. In particular, McMillan-Rowell resonances require the occurrence of Andreev reflections at the YBCO/LCMO interface, and the coherent propagation

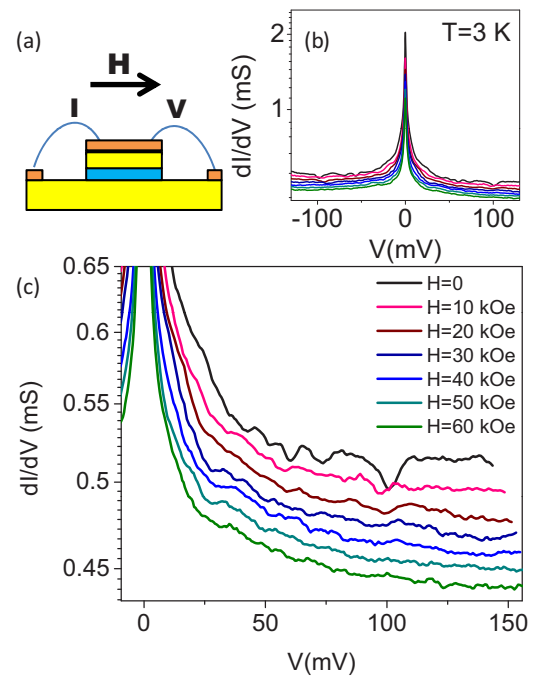


FIG. 3. (Color online) (a) Sketch of the vertical junction and applied field direction. (b) Differential conductance across a Au/YBCO (15 nm)/LCMO (12 nm)/YBCO (30 nm)/STO// junction (area  $32 \mu\text{m}^2$ ), measured at  $T = 3$  K for different magnetic field applied parallel to the film plane. (c) Zoom of the curves shown in (b).

of the resulting electron-hole pairs across the entire LCMO layer [9]—whose thickness ranges between 9 and 30 nm in the different samples. In the experiments discussed here, we study how the conductance features change as a function of the applied magnetic field and of the LCMO macroscopic magnetization. The measurements were carried either in a He flow cryostat equipped with a 5.7 kOe electromagnet or in a liquid He cryostat equipped with a 70 kOe superconducting coil. The magnetic field influence on the spectral features was studied at our equipment base temperature ( $\sim 3$  K), since the spectral features smooth away as temperature is increased (see temperature dependent studies in Ref. [9]).

Figure 1(c) shows measurements for a YBCO (15 nm)/LCMO (30 nm) bilayer, in the absence of magnetic field (black top curve) and under application of  $H = 5.7$  kOe perpendicular to the film plane (red lower curve). Note that, in the main panel, the curves have been vertically displaced for clarity. The original data are displayed in the inset. The latter shows that the overall conductance is very weakly affected by the application of the magnetic field. The inspection of the main panel evidences that the sole effect of the applied field is a minimal smoothing of the conductance features. No significant shift of the resonances is observed along the  $x$  axis. In order to determine the effect of the applied field on the LCMO magnetization, we measured the hysteresis loop of a plain 15-nm-thick LCMO film on STO, using a superconducting quantum interference device magnetometer with the field applied perpendicular to the film plane [Fig. 1(b)]. From this measurement, we learn that the LCMO magnetization is not fully saturated under the applied field  $H = 5.7$  kOe; however, this field produces a significant change of the macroscopic magnetization with respect to that at  $H = 0$ . In conclusion, the measurements shown in Fig. 1 show that sizable changes of the macroscopic magnetization—induced by moderate perpendicular fields—lead to very minor changes of the junction’s conductance. This is in stark contrast with the results reported by Kalcheim *et al.* [19]: in their STM experiments, the spectral features that constitute the fingerprint of long-range proximity effects significantly varied under the application of moderate (a few kOe) perpendicular magnetic fields.

Figure 2 displays measurements with the magnetic field applied in plane. This junction is based on a YBCO (15 nm)/LCMO (12 nm)/YBCO (30 nm) heterostructure which, as discussed earlier [9], shows the same conductance behavior as YBCO/LCMO bilayers. As can be seen in Fig. 2(c), the conductance for  $H = 0$  and  $H = 5.7$  kOe (in plane) are identical within the experimental resolution. Figure 2(b) displays the magnetization loop for a plain LCMO/YBCO plain film with similar LCMO thickness as the measured junction. Note that saturation of the LCMO macroscopic magnetization occurs around  $H \sim 1.5$  kOe. In consequence, during conductance measurement at  $H = 5.7$  kOe the LCMO magnetization is fully saturated in plane.

To summarize the experimental findings of Figs. 1 and 2: in the presence of moderate fields (i) the conductance shows very minor changes, if any, as compared to the case  $H = 0$ ; and (ii) the conductance is independent of the macroscopic magnetization of the LCMO layer, and in particular on whether

this is completely saturated (or not) in the in-plane/out-of-plane directions.

The effect of stronger magnetic fields is shown in Fig. 3. Figure 3(b) shows a series of conductance curves for increasing in-plane fields, from  $H = 0$  to  $H = 60$  kOe. In Fig. 3(c), a zoom of the same curves around positive bias is shown. In addition to a gradual decrease of the background conductance, one can see that the conductance resonances progressively fade away as the applied field is increased. Thus, although a few kOe fields do not have clear effects on the conductance curves (Figs. 1 and 2), higher fields progressively wash away the fingerprints of long-range proximity effect (Fig. 3).

Let us now interpret the experimental results. The invariance of the conductance measurements for low magnetic fields, and in particular the fact that the conductance features do not depend on the LCMO macroscopic magnetization, implies that “bulk” inhomogeneities such as domain walls—theoretically proposed as a possible source of triplet generation in  $c$ -axis cuprate/F systems [39]—do not play a role in the present experiments. Note in particular that, both for perpendicular [Fig. 1(b)] and parallel applied fields [Fig. 2(b)], a very different magnetic domain structure is expected between remanence ( $H = 0$ ) and at  $H = 5.7$  kOe. Yet, no significant differences exist between the respective (black/red) conductance curves [either in Fig. 1(c) or in Fig. 2(c)]. The minor smoothing in the case of perpendicular applied field [Fig. 1(b)] may arise from vortex nucleation effects, which are expected when the magnetic field is applied perpendicular to the YBCO film.

Conversely, the strong changes of the conductance features upon application of large *in-plane* magnetic fields (Fig. 3) are unlikely due to artifacts associated with vortex nucleation, since the YBCO layer thickness is much smaller than the London penetration depth along the  $c$  axis ( $\sim 800$  nm). Those spectral changes are also inconsistent with a field-induced depression of the superconducting order parameter (energy gap  $\Delta$ ). On the one hand, this would be unexpected since the applied fields range is much below the YBCO critical field at that temperature. Furthermore, should the field depression of superconductivity play a role, and provided that the position of the Tomesch resonances depend on  $\Delta$  [38], one would expect a gradual, sizable shift of the conductance oscillations towards lower energies as they fade away, which is not observed. In conclusion, the magnetic field effect on the superconductor cannot explain the spectral changes observed in Fig. 3. These changes must be due to the magnetic field effect on the LCMO. More specifically, and considering that the macroscopic magnetization is fully saturated within the range for which field effects are observed, the field-induced spectral changes must be due to changes of the magnetic structure at the YBCO/LCMO interface.

Different types of magnetic inhomogeneities at the  $c$ -axis YBCO/LCMO interface are known which are sensitive to fields in the tens of kOe:

(a) On the LCMO side, the magnetization is depressed due to a doping effect caused by electron transfer from the LCMO to the YBCO. The charge transfer (nearly 0.2 electrons per atomic plane) results from the difference in the electrochemical potentials between both materials [40,41]. As a result, the boundary between ferromagnetic and antiferromagnetic phases is approached and the ferromagnetism of the LCMO is

depressed at the interface as has been experimentally observed through polarized neutron reflectometry experiments [33]. This type of interfacial magnetic inhomogeneity results from the known tendency of the La/Ca manganite to phase separation for doping levels in the vicinity of the boundary between different phases. A strong magnetic field may tip the balance between ferromagnetic and nonferromagnetic phases, thereby canceling part of the magnetic inhomogeneity. This is consistent with the observed magnetic field dependence.

(b) On the other hand, in the YBCO side, uncompensated Cu moments exist due to the strong antiferromagnetic superexchange between Mn and Cu at the interfacial Mn-O-Cu bonds. This interaction yields a net Cu moment, which results from tilting of the interface Cu sublattice [42]—otherwise antiferromagnetic due to the hole count reduction induced by the charge transfer. Although the effective exchange field on the interfacial Cu moments is very large ( $\sim 1000$  kOe), it decays over  $\sim 2 - 3$  unit cells, as determined by the hopping rate along the  $c$  axis [43]. Thus, the extent of the inhomogeneity (Cu canting) could be modulated upon application of fields in the  $\sim$ tens of kOe. Furthermore, these fields should also affect the Cu exchange field inhomogeneities through the alignment the Mn moments at the interface.

In conclusion, and contrary to the behavior reported in  $a$ -axis YBCO/LCMO interfaces, we have found that in  $c$ -axis YBCO/LCMO interfaces the conductance features that evidence long-range proximity effects are essentially insensitive to moderate magnetic fields, and independent of the macroscopic magnetization within the LCMO layer. However, the spectral fingerprints of the long-range proximity effect fade away for magnetic fields well above the magnetic LCMO saturation field. This is consistent with the idea that the known sources of inhomogeneous magnetization at both sides of the  $c$ -axis YBCO/LCMO interface, which appear due to electronic reconstruction and are sensitive to magnetic fields within that range, play a role in the generation of long-range proximity effects.

Work at the Unité Mixte de Physique CNRS/Thales was supported by the French ANR (Contract JCJC “SUPERHYBRIDS-II”) and FP7 Marie Curie Actions “PIXIE.” Research at UCM was supported by Spanish MINECO through Grant No. MAT2014-52405-C02-01. J.S. acknowledges the CNRS “Institut de Physique” for supporting his visiting position at the Unité Mixte de Physique CNRS/Thales.

- 
- [1] A. I. Buzdin, *Rev. Mod. Phys.* **77**, 935 (2005).
- [2] F. S. Bergeret, A. F. Volkov, and K. B. Efetov, *Phys. Rev. Lett.* **86**, 4096 (2001).
- [3] R. S. Keizer, S. T. B. Goennenwein, T. M. Klapwijk, G. Miao, G. Xiao, and A. Gupta, *Nature (London)* **439**, 825 (2006).
- [4] M. S. Anwar, F. Czeschka, M. Hesselberth, M. Porcu, and J. Aarts, *Phys. Rev. B* **82**, 100501 (2010).
- [5] T. S. Khaire, M. A. Khasawneh, W. P. Pratt, Jr., and N. O. Birge, *Phys. Rev. Lett.* **104**, 137002 (2010).
- [6] D. Sprungmann, K. Westerholt, H. Zabel, M. Weides, and H. Kohlstedt, *Phys. Rev. B* **82**, 060505 (2010).
- [7] J. W. A. Robinson, J. D. S. Witt, and M. G. Blamire, *Science* **329**, 59 (2010).
- [8] Y. Kalcheim, T. Kirzhner, G. Koren, and O. Millo, *Phys. Rev. B* **83**, 064510 (2011).
- [9] C. Visani, Z. Sefrioui, J. Tornos, C. Leon, J. Briatico, M. Bibes, A. Barthélémy, J. Santamaría, and J. E. Villegas, *Nat. Phys.* **8**, 539 (2012).
- [10] M. Eschrig, *Phys. Today* **64**(1), 43 (2011).
- [11] M. Eschrig and T. Löfwander, *Nat. Phys.* **4**, 138 (2008).
- [12] P. A. Kraus, A. Bhattacharya, and A. M. Goldman, *Phys. Rev. B* **64**, 220505(R) (2001).
- [13] Z. Y. Chen, A. Biswas, I. Žutić, T. Wu, S. B. Ogale, R. L. Greene, and T. Venkatesan, *Phys. Rev. B* **63**, 212508 (2001).
- [14] Z. Sefrioui, D. Arias, V. Peña, J. E. Villegas, M. Varela, P. Prieto, C. León, J. L. Martínez, and J. Santamaría, *Phys. Rev. B* **67**, 214511 (2003).
- [15] P. S. Luo, H. Wu, F. C. Zhang, C. Cai, X. Y. Qi, X. L. Dong, W. Liu, X. F. Duan, B. Xu, L. X. Cao, X. G. Qiu, and B. R. Zhao, *Phys. Rev. B* **71**, 094502 (2005).
- [16] K. Dybko, K. Werner-Malento, P. Aleshkevych, M. Wojcik, M. Sawicki, and P. Przyslupski, *Phys. Rev. B* **80**, 144504 (2009).
- [17] M. van Zalk, A. Brinkman, J. Aarts, and H. Hilgenkamp, *Phys. Rev. B* **82**, 134513 (2010).
- [18] I. Fridman, L. Gunawan, G. A. Botton, and J. Y. T. Wei, *Phys. Rev. B* **84**, 104522 (2011).
- [19] Y. Kalcheim, I. Felner, O. Millo, T. Kirzhner, G. Koren, A. Di Bernardo, M. Egilmez, M. G. Blamire, and J. W. A. Robinson, *Phys. Rev. B* **89**, 180506 (2014).
- [20] V. Peña, Z. Sefrioui, D. Arias, C. Leon, J. L. Martínez, and J. Santamaría, *Eur. Phys. J. B* **40**, 479 (2004).
- [21] M. Egilmez, J. W. A. Robinson, J. L. MacManus-Driscoll, L. Chen, H. Wang, and M. G. Blamire, *Europhys. Lett.* **106**, 37003 (2014).
- [22] A. F. Volkov, F. S. Bergeret, and K. B. Efetov, *Phys. Rev. Lett.* **90**, 117006 (2003).
- [23] M. Houzet and A. I. Buzdin, *Phys. Rev. B* **76**, 060504(R) (2007).
- [24] J. Linder, T. Yokoyama, and A. Sudbø, *Phys. Rev. B* **79**, 054523 (2009).
- [25] Y. Asano, Y. Sawa, Y. Tanaka, and A. A. Golubov, *Phys. Rev. B* **76**, 224525 (2007).
- [26] K. Halterman and O. T. Valls, *Phys. Rev. B* **80**, 104502 (2009).
- [27] J. Linder, M. Cuoco, and A. Sudbø, *Phys. Rev. B* **81**, 174526 (2010).
- [28] A. S. Mel’nikov, A. V. Samokhvalov, S. M. Kuznetsova, and A. I. Buzdin, *Phys. Rev. Lett.* **109**, 237006 (2012).
- [29] Z. P. Niu, *Europhys. Lett.* **100**, 17012 (2012).
- [30] F. S. Bergeret, A. Verso, and A. F. Volkov, *Phys. Rev. B* **86**, 214516 (2012).
- [31] F. S. Bergeret and I. V. Tokatly, *Phys. Rev. Lett.* **110**, 117003 (2013).
- [32] V. Peña, Z. Sefrioui, D. Arias, C. Leon, J. Santamaría, M. Varela, S. J. Pennycook, and J. L. Martínez, *Phys. Rev. B* **69**, 224502 (2004).
- [33] A. Hoffmann, S. G. E. te Velthuis, Z. Sefrioui, J. Santamaría, M. R. Fitzsimmons, S. Park, and M. Varela, *Phys. Rev. B* **72**, 140407(R) (2005).

- [34] T. Hu, H. Xiao, C. Visani, J. Santamaria, and C. C. Almasan, *New J. Phys.* **13**, 033040 (2011).
- [35] Y. Liu, C. Visani, N. M. Nemes, M. R. Fitzsimmons, L. Y. Zhu, J. Tornos, M. Garcia-Hernandez, M. Zhernenkov, A. Hoffmann, C. Leon, J. Santamaria, and S. G. E. te Velthuis, *Phys. Rev. Lett.* **108**, 207205 (2012).
- [36] W. McMillan and P. Anderson, *Phys. Rev. Lett.* **16**, 85 (1966).
- [37] J. Rowell and W. McMillan, *Phys. Rev. Lett.* **16**, 453 (1966).
- [38] W. J. Tomasch, *Phys. Rev. Lett.* **16**, 16 (1966).
- [39] A. F. Volkov and K. B. Efetov, *Phys. Rev. Lett.* **102**, 077002 (2009).
- [40] M. Varela, A. R. Lupini, S. J. Pennycook, Z. Sefrioui, and J. Santamaria, *Solid-State Electron.* **47**, 2245 (2003).
- [41] J. Salafranca, J. Rincón, J. Tornos, C. León, J. Santamaria, E. Dagotto, S. J. Pennycook, and M. Varela, *Phys. Rev. Lett.* **112**, 196802 (2014).
- [42] J. Chakhalian, J. W. Freeland, G. Srajer, J. Stempfer, G. Khaliullin, J. C. Cezar, T. Charlton, R. Dalgliesh, C. Bernhard, G. Cristiani, H. U. Habermeier, and B. Keimer, *Nat. Phys.* **2**, 244 (2006).
- [43] J. Salafranca and S. Okamoto, *Phys. Rev. Lett.* **105**, 256804 (2010).